ACS APPLIED MATERIALS & INTERFACES

Research Article

www.acsami.org

Effects of ZnO Nanoparticles on P3HT:PCBM Organic Solar Cells with DMF-Modulated PEDOT:PSS Buffer Layers

Sang Hoon Oh, Seung Jin Heo, Jeong Suk Yang, and Hyun Jae Kim*

School of Electrical and Electronic Engineering, Yonsei University, 50 Yonsei-ro, Seodaemun-gu, Seoul 120-749, Korea

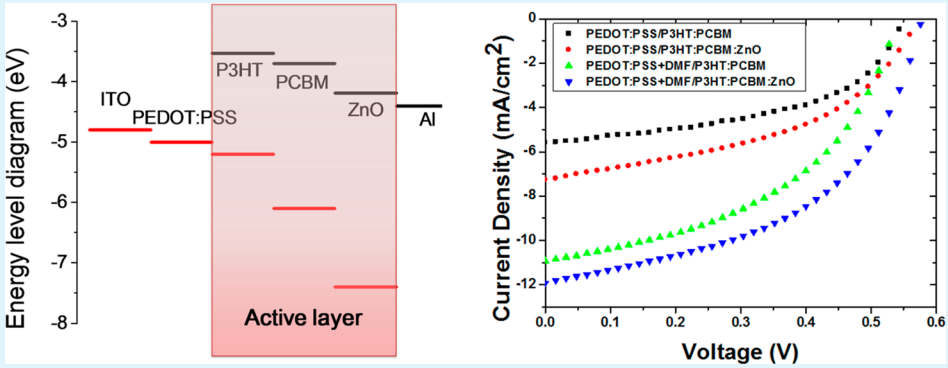

ABSTRACT: In this study, we investigated hybrid bulk heterojunction organic solar cells containing ZnO nanoparticles blended with poly(3-hexylthiophene) (P3HT) and phenyl-C_{61}-butyric acid methyl ester (PCBM) and having poly(3,4-ethylenedioxythiophene) poly(styrenesulfonate) (PEDOT:PSS) or *N*,*N*-dimethylformamide (DMF)-modulated PEDOT:PSS buffer layers. The reference cell, which had a P3HT:PCBM active layer sandwiched between ITO\PEDOT:PSS and LiF\Al electrodes, exhibited an efficiency of 1.55%. The ZnO nanoparticle-doped active layer (ITO\PEDOT:PSS(DMF) \ZnO:P3HT:PCBM\LiF \Al) exhibited a higher efficiency of 3.39% due to the modulated PEDOT:PSS buffer layer with low resistivity and the hybrid active layer containing ZnO nanoparticles. Here, we demonstrate that the low resistivity of the PEDOT:PSS layer can improve the J_{sc} value of hybrid solar cells, and ZnO nanoparticles can enhance the V_{oc} value of organic solar cells.

KEYWORDS: *ZnO nanoparticle, hybrid solar cell, DMF-modulated PEDOT:PSS*

1. INTRODUCTION

Organic solar cells based on bulk heterojunctions (BHJs) have been investigated because of their low cost, environmentally friendly production, ease of deposition, and flexible applications.[1−3] The advantages of BHJ organic solar cells are attracting attention for applications in next-generation solar cells. BHJ solar cells based on poly(3-hexylthiophene) (P3HT) as the electron donor and (6.6) phenyl-C_{61}-butyric acid methyl ester (PCBM) as the electron acceptor have exhibited power conversion efficiencies (PCEs) higher than 3% under AM 1.5 G illumination.[4,5] The PCEs of BHJ organic solar cells can be enhanced by controlling various factors, such as donor/acceptor materials,[6,7] buffer layers,[8] annealing temperature,[9,10] and electrode materials.[11]

The hybrid active layer of polymers conjugated with inorganic semiconductor nanoparticles has been intensively researched to improve the efficiency of solar cells.[12−16] These hybrid active layers have the advantage of high electron mobility due to the inorganic semiconductor materials. Olson et al. investigated the performance of CdSe with various capping ligands[12] and reported an efficiency of about 1.8% for the CdSe-blended hybrid active layer. The efficiencies of TiO_2 nanoparticles,[13] PbS,[14] CdSe,[15] and PbSe[16] are reportedly 1.71, 1.3, 2.0, and 0.14%, respectively. To date, several studies have reported the incorporation of ZnO into P3HT active layers.[17−19] Olson et al.[19] obtained the highest efficiency of 2.03%. The enhanced performance of the organic solar cell was attributed to bandgap extraction of the BHJ with ZnO nanoparticles in the hybrid active layer and to improved electron mobility.

It is important to decrease the resistivity of PEDOT:PSS films because generated holes can move easily to the metal electrode. Many approaches have been used to decrease the resistivity of PEDOT:PSS film using *N*,*N*-dimethyl formamide (DMF),[20] glycerol,[21] diethylene glycol,[22] and dimethyl sulfoxide.[23] Low-resistivity PEDOT:PSS films are used to enhance the PCE of organic solar cells, but the benefit of using low-resistivity modulated PEDOT:PSS films is not clear.

In this study, we investigated the incorporation of ZnO nanoparticles in photoactive layers of organic solar cells and DMF-modulated PEDOT:PSS in the hole-transporting layer. Methods for controlling the active and hole-transporting layers could improve the electrical properties of BHJ organic solar

Received: March 31, 2013
Accepted: October 31, 2013
Published: October 31, 2013

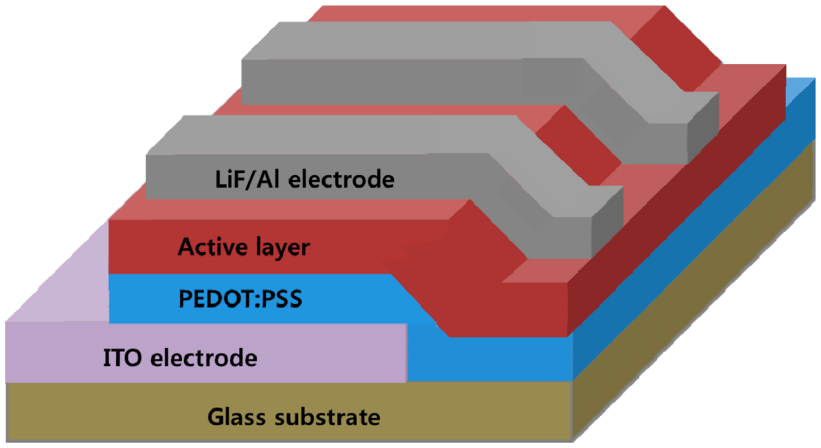

Figure 1. Structure of organic and ZnO nanoparticle-doped hybrid solar cell.

cells, resulting in high open circuit voltage (V_{oc}) and high short circuit current density (J_{sc}).

2. EXPERIMENTAL PROCEDURE

Material. PEDOT:PSS solution modulated with DMF was mixed at a volume ratio of 7:3 ((PEDOT:PSS):DMF). The mixed solution was stirred with a magnetic stirrer for 1 h at room temperature. To prepare the ZnO nanoparticle solution, commercial ZnO nanoparticles (Sigma-Aldrich, <100 nm diameter) were dissolved in methanol at 10 mg/mL, followed by stirring for 1 h in a nitrogen-filled glovebox. To compare the organic active layer with the hybrid layer, the prepared ZnO nanoparticle solution and the organic materials, dissolved at volume ratio of 1:40, were stirred for 1 h in a glovebox.

Hybrid Solar Cell Fabrication. The photovoltaic devices were prepared on indium tin oxide (ITO) (~150 nm) substrates with 7 Ω/□ of sheet resistance. The ITO substrates were cleaned in an ultrasonic bath with acetone, methanol, and deionized water for 15 min and dried with a nitrogen gun. To fabricate the hole-transporting layers, pristine PEDOT:PSS and DMF-modulated PEDOT:PSS solutions were filtered with 0.45 um syringe filters, deposited by spin coating at 3000 rpm for 30 s and baked at 150 °C in air. As a pristine active layer, a solution of P3HT and PCBM was prepared at a 1:0.8 ratio in chlorobenzene solution (15 mg/mL). ITO\PEDOT:PSS \P3HT:PCBM\LiF\Al was fabricated as the reference cell, as shown in Figure 1. P3HT:PCBM solution was deposited as an active layer on a patterned ITO\PEDOT:PSS layer by spin coating and annealed at 120 °C for 10 min in a glovebox. LiF and Al electrodes (150 nm thick) were deposited with a metal shadow mask by thermal evaporation on the active layer in a high-vacuum system at an evaporation rate of 0.8–1.2 Å/s. The area of the active layer was 4 mm^2.

The P3HT:PCBM:ZnO mixed solution was deposited by spin coating and then heated at 120 °C on a hot plate for 10 min in a glovebox. The thicknesses of the pristine active layer and hybrid active layer were measured using a surface profiler (Tencor, Alpha step). The two layers had nearly the same thickness (150 nm). The top electrodes were deposited under the same conditions described for the reference cells. After deposition, the pristine cell and hybrid cell were postannealed at 120 °C for 10 min in a glovebox. Figure 1 presents the detailed structure of the organic solar cell: the structure is typical for wet-etched ITO electrodes. The thicknesses of the pristine and modulated PEDDOT:PSS layers were almost the same (~30 nm), and the thicknesses of the active and hybrid layers were approximately 150 nm. LiF\Al (100 nm) was used as a cathode in the solar cells.

The resistivity of each PEDOT:PSS film was measured using the Hall technique in the van der Pauw configuration (HMS-3000, Ecopia). The electrical properties of the solar cells were measured under a white-light halogen lamp set to AM 1.5 G at 100 mW/cm^2. To investigate the morphology of the active layer, surface analysis of the thin films was performed using an atomic force microscope (AFM, XE-150, Park Systems) in noncontact mode. To investigate the optical properties of the active layers, the transparency of each thin film was measured using an ultraviolet–visible spectrophotometer (UV–vis, V-650, JASCO).

3. RESULTS AND DISCUSSION

Figure 2 presents the energy band diagram proposed for the ZnO-conjugated hybrid solar cell. The work function of DMF-

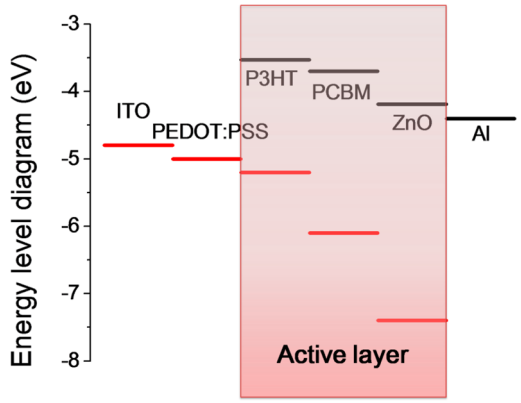

Figure 2. Schematic diagram of the band diagram for ZnO nanoparticles in the active layer.

modulated PEDOT:PSS was almost the same as that for pristine PEDOT:PSS films.[20] The lowest unoccupied molecular orbital (LUMO) and highest occupied molecular orbital (HOMO) levels of P3HT are −3.53 and −5.2 eV, respectively.[17] The LUMO and HOMO energy levels of PCBM are −3.7 and −6.1 eV, respectively.[17] The conduction energy level of ZnO nanoparticle is −4.19 eV.[18] The work functions of PEDOT:PSS and Al are −4.9 and −4.3 eV,[24] respectively. The conduction energy level of ZnO nanoparticles is similar to that of Al thin film. As shown in Figure 2, photogenerated electron–hole pairs are produced at the interfaces of P3HT and PCBM. Generated holes are transported to the ITO electrode through the PEDOT:PSS buffer layer. ZnO nanoparticles in the hybrid active layer help transport electron carriers to the cathode because of their higher electron mobility and lower conduction energy level in the hybrid active layer. Generated electrons cannot be transported to the ITO anode because of PEDOT:PSS hole transporting layer. As a result, the performance of the device was improved by conjugating ZnO nanoparticles with the

organic active layer and this hybrid active layer could enhance electron transportation to cathode.

To improve the electrical properties of the PEDOT:PSS hole-transporting layer, DMF was added to PEDOT:PSS solution. The resistivity of the pristine PEDOT:PSS film was 7.87×10^{-1} Ω·cm, and the resistivity of the DMF-modulated PEDOT:PSS film decreased to 1.45×10^{-2} Ω·cm. The reduced resistivity did not result from the screening effect due to interactions between ions and charge carriers in the solvent, which would be progressive, but rather from phase separations of PEDOT and PSS.[22] The dipole moment of DMF is 3.86 D, and this relatively high dipole moment could affect positively charged PEDOT segments in PEDOT:PSS films. This DMF solvent significantly increased the conductivity by increasing the probability that carriers would be transported through the conductive pathway without being recombined or trapped in the thin-film.[25] Thus, the DMF-modulated PEDOT:PSS film exhibited lower resistivity due to an increased probability that carriers would be transported through the conductive pathway without being recombined or trapped in the thin film. The conduction mechanism could explain the high J_{sc} value for the organic solar cells having a DMF-modulated PEDOT:PSS hole-transporting layer with lower resistivity than the pristine layer.

Figure 3 presents the $J-V$ characteristic curves of the P3HT:PCBM and ZnO:P3HT:PCBM solar cells on pristine or

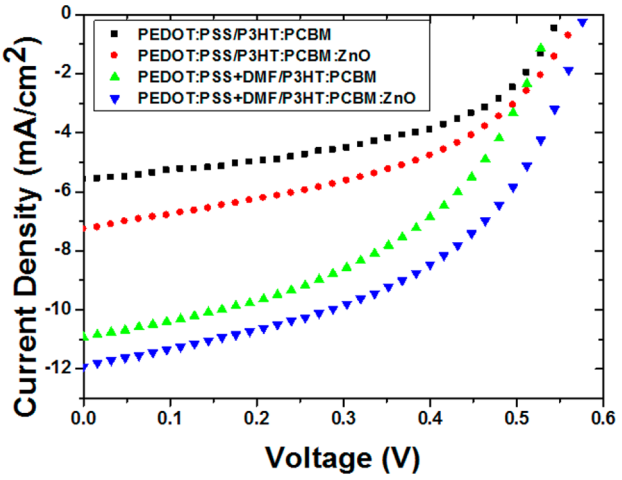

Figure 3. Current–voltage characteristics of P3HT:PCBM and ZnO:P3HT:PCBM thin films with PEDOT:PSS and DMF-modulated PEDOT:PSS.

DMF-modulated PEDOT:PSS buffer layers under A.M. 1.5 G illuminations with an intensity of 100 mW/cm^2. Table 1 summarizes the electrical properties of all the devices. The performances of the photovoltaic devices were highly dependent on the PEDOT:PSS buffer layers and ZnO nanoparticle-doped active layer. For the reference cell, the organic solar cell with a pristine PEDOT:PSS buffer layer and P3HT:PCBM active layer exhibited an efficiency as high as 1.55%. When active layer was doped with ZnO nanoparticles, V_{oc} and J_{sc} were slightly increased. Hybrid active layer could enhance generated electron transportation to cathode due to the high electron mobility of ZnO nanoparticles in active layer. Furthermore, there are contributions from the heterojunction electric field formed between ZnO and organic materials since this electric field will be propitious to the separation of the electron–hole pairs and hence results in the increase of the photoelectric conversion property. This role of ZnO nanoparticles increased the solar cell performance than P3HT:PCBM pristine organic solar cells. The DMF-modulated PEDOT:PSS buffer layer was crucial for improving the performance of solar cell devices with high J_{sc} values, as shown in Figure 3. It is clear that the DMF-modulated PEDOT:PSS buffer layer can increase the J_{sc} value of the cells due to its low resistivity. For organic solar cells having a DMF-modulated PEDOT:PSS buffer layer, the J_{sc} was 10.91 mA/cm^2, the V_{oc} was 0.541 V, the fill factor (FF) was 47.12%, and the PCE was 2.78%. When ZnO nanoparticles were doped in the P3HT:PCBM active layer, V_{oc} increased slightly, relative to the reference cells. Similar to the ZnO-doped P3HT:PCBM active layer, the DMF-modulated PEDOT:PSS buffer layer can generate higher J_{sc} values than the pristine PEDOT:PSS buffer layer. Therefore, we expected the best performance when DMF-modulated PEDOT:PSS was the hole-transporting layer and ZnO nanoparticle-doped P3HT:PCBM was the active layer. In this case, the device performance of hybrid organic solar cells was J_{sc} = 11.91 mA/cm^2, V_{oc} = 0.579 V, and FF = 49.28%, resulting in PCE = 3.39%.

To investigate the effects of ZnO nanoparticles on the active layer, we applied atomic force microscopy (AFM) and UV–visible absorption spectroscopy to the P3HT:PCBM film and the ZnO nanoparticle-doped P3HT:PCBM film. The AFM images clearly revealed that addition of ZnO nanoparticles into the active layer increased the roughness of the films (Figure 4 (a) and (b)). RMS roughness of pristine P3HT:PCBM layer was 1.22 nm, and ZnO nanoparticles conjugated hybrid layer was 5.67 nm. When ZnO nanoparticles were doped into the P3HT:PCBM film, the surface was rougher than that of the pristine P3HT:PCBM film due to the large size of the ZnO nanoparticles. This roughness of the ZnO:P3HT:PCBM film surface resulted in greater light absorption due to the diffuse reflection between the active layer and the top electrode.

Figure 5 shows the UV–visible absorption spectra of P3HT:PCBM and ZnO:P3HT:PCBM thin films on glass. The UV–visible spectrum of the P3HT:PCBM organic film had two large peaks: the first appeared near 513 nm, corresponding to poly thiophene; the second appeared at 335 nm, corresponding to the fullerene C_{60} derivative. Because thickness of active layer was similar, ZnO nanoparticles influenced the absorption in active layer. As mentioned before, roughness of active layer was increased when ZnO nanoparticles was mixed with organic active materials. The rougher film surface could reflect more light between active layer and

Table 1. Electrical Properties of Hybrid Solar Cells

	V_{oc} (V)	J_{sc} (mA/cm^2)	FF (%)	eff (%)
PEDOT:PSS\P3HT:PCBM	0.551	5.58	50.68	1.55
PEDOT:PSS\P3HT:PCBM:ZnO	0.574	7.27	45.91	1.91
PEDOT:PSS(DMF)\P3HT:PCBM	0.541	10.93	47.12	2.78
PEDOT:PSS(DMF)\P3HT:PCBM:ZnO	0.579	11.91	49.28	3.39

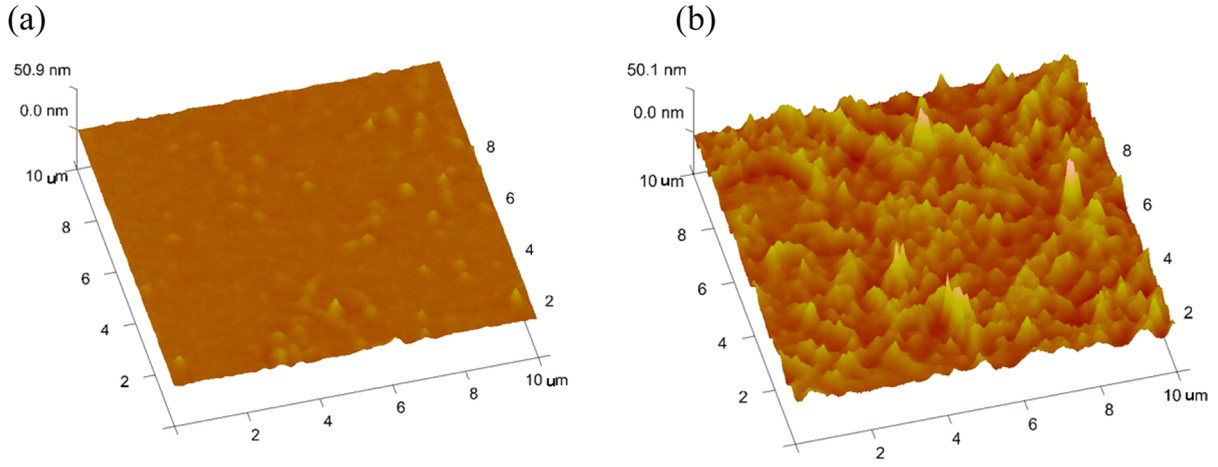

Figure 4. AFM images of (a) P3HT:PCBM and (b) ZnO:P3HT:PCBM surfaces.

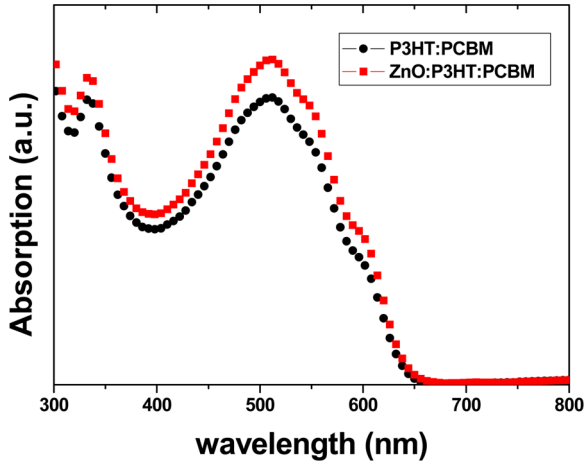

Figure 5. Optical absorption spectra of P3HT:PCBM and ZnO:P3HT:PCBM thin films.

metal cathode. For this reason, the absorption spectra of the ZnO:P3HT:PCBM film was slightly higher than that of the P3HT:PCBM film in the range of 300−560 nm.

4. CONCLUSIONS

Hybrid BHJ solar cells have been successfully processed from solution by doping ZnO nanoparticles in a P3HT:PCBM active layer and using a DMF-modulated PEDOT:PSS buffer layer as a hole-transporting layer. ZnO nanoparticles conjugated active layer increased the V_{oc} value of the organic solar cells. And the low resistivity of the DMF-modulated PEDOT:PSS buffer layer significantly increased the J_{sc} value of the organic solar cells. The corresponding photovoltaic devices exhibited improved photocurrent, open-circuit voltage, and fill factor, leading to a PCE of 3.39% under illumination at 100 mW/cm^2. The combination of the two methods used in this study to improve the performance of organic solar cells resulted in higher efficiency compared to the conventional fabrication process.

AUTHOR INFORMATION

Corresponding Author

*E-mail: hjk3@yonsei.ac.kr.

Notes

The authors declare no competing financial interest.

ACKNOWLEDGMENTS

This work was supported by the National Research Foundation of Korea (NRF) grant funded by the Korean Ministry of Education, Science and Technology (MEST) [no. 2011-0028819].

REFERENCES

(1) Yu, G.; Gao, J.; Hummelen, J. C.; Wudl, F.; Heeger, A. J. *Science* **1995**, *270*, 1789−1791.
(2) Krebs, F. C.; Alstrup, J.; Spanggaard, H.; Larsen, K.; Kold, E. *Sol. Energy Mater. Sol. Cells* **2004**, *83*, 293−300.
(3) Dennler, G.; Lungenschmied, C.; Neugebauer, H.; Sariciftic, N. S.; Labouret, A. *J. Mater. Res.* **2005**, *20*, 3224−3233.
(4) Reyes-Reyes, M.; Kim, K.; Dewald, J.; Lopez-Sandoval, R.; Avadhanula, A.; Curran, S.; Carroll, D. L. *Org. Lett.* **2005**, *7*, 5749−5752.
(5) Ma, W. L.; Yang, C. Y.; Gong, X.; Lee, K.; Heeger, A. J. *Adv. Funct. Mater.* **2005**, *15*, 1617−1622.
(6) Brabec, C. J.; Sariciftci, N. S.; Hummelen, J. C. *Adv. Funct. Mater.* **2001**, *11*, 15−26.
(7) Yun, D.; Feng, W.; Wu, H.; Yoshino, K. *Sol. Energy Mater. Sol. Cells* **2009**, *93*, 1208−1213.
(8) Waldauf, C.; Morana, M.; Denk, P.; Schilinsky, P.; Coakley, K.; Choulis, S. A.; Brabec, C. J. *Appl. Phys. Lett.* **2006**, *89*, 233517.
(9) Inoue, K.; Ulbricht, R.; Madakasira, P. C.; Sampson, W. M.; Lee, S.; Gutierrez, J.; Ferraris, J.; Zakhidov, A. A. *Synth. Met.* **2005**, *154*, 41−44.
(10) Li, G.; Shrotriya, V.; Yao, Y.; Yang, Y. *J. Appl. Phys.* **2005**, *98*, 043704.
(11) Reese, M. O.; White, M. S.; Rumbles, G.; Ginley, D. S.; Shaheen, S. E. *Appl. Phys. Lett.* **2008**, *92*, 053307.
(12) Olson, J. D.; Gray, G. P.; Carter, S. A. *Sol. Energy Mater. Sol. Cells* **2009**, *93*, 519−523.
(13) Lin, Y.; Wei, Q.; Qian, G.; Yao, L.; Watkins, J. J. *Macromolecules* **2012**, *45*, 8665−8673.
(14) Zhao, N.; Osedach, T. P.; Chang, L.-Y.; Geyer, S. M.; Wanger, D.; Binda, M. T.; Arango, A. C.; Bawend, M. G.; Bulovic, V. *ACS Nano* **2010**, *4*, 3743−3752.
(15) Radychev, N.; Lokteva, I.; Witt, F.; Kolny-Olesiak, J.; Borchert, H.; Parisi, J. *J. Phys. Chem. C* **2011**, *115*, 14111−14122.
(16) Yun, D.; Feng, W.; Wu, H.; Yoshino, K. *Sol. Energy Mater. Sol. Cells* **2009**, *93*, 1208−1213.
(17) Wang, M.; Wang, X. *Sol. Energy Mater. Sol. Cells* **2008**, *92*, 766−771.
(18) Beek, W. J. E.; Wienk, M. M.; Janssen, R. A. J. *Adv. Funct. Mater.* **2006**, *16*, 1112−1116.
(19) Olson, D. C.; Piris, J.; Collins, R. T.; Shaheen, S. E.; Ginley, D. S. *Thin solid films* **2006**, *496*, 26−29.

(20) Kim, K. M.; Lee, K. W.; Moujoud, A.; Oh, S. H.; Kim, H. J. *Electrochem. Solid-State Lett.* **2010**, *13*, H447−H449.
(21) Zhang, F.; Johansson, M.; Andersson, M. R.; Hummelen, J. C.; Inganas, O. *Adv. Funct. Mater.* **2002**, *14*, 662−665.
(22) Crispin, X.; Jakobsson, F. L. E.; Crispin, A.; Grim, P. C. M.; Andersson, P.; Volodin, A.; van Haesendonck, C.; Van der Auweraer, M.; Salaneck, W. R. *Chem. Mater.* **2006**, *18*, 4354−4360.
(23) Closmann, A.; Stenzel, F.; Balthasar, G.; Do, H.; Lemmer, U. *Thin solid films* **2009**, *517*, 1750−1752.
(24) Choi, M.-R.; Han, T.-H.; Lim, K.-G.; Woo, S.-H.; Huh, D. H.; Lee, T.-W. *Angew. Chem.* **2011**, *123*, 6398−6401.
(25) Yang, J. S.; Oh, S. H.; Kim, D. L.; Kim, S. J.; Kim, H. J. *ACS Appl. Mater. Interfaces* **2012**, *4*, 5394−5398.